Flow effects on silicate dissolution and ion transport at an aqueous interface

Journal:	*Physical Chemistry Chemical Physics*
Manuscript ID	CP-ART-02-2019-000640.R1
Article Type:	Paper
Date Submitted by the Author:	02-Mar-2019
Complete List of Authors:	Lian, Cheng; East China University of Science and Technology, KONG, Xian; Institution of Biochemical Engineering, Department of Chemical Engineering Liu, Honglai; East China University of Science and Technology, Wu, Jianzhong; University of California, Riverside, Chemical and Environmental Engineering

Flow effects on silicate dissolution and ion transport at an aqueous interface

Cheng Lian[1,2], Kong Xian[3], Honglai Liu[1*], and Jianzhong Wu[2*]

[1] State Key Laboratory of Chemical Engineering, and School of Chemistry and Molecular Engineering, East China University of Science and Technology, Shanghai, 200237, P. R. China

[2] Department of Chemical and Environmental Engineering, University of California, Riverside, CA 92521, USA

[3]Department of Chemical Engineering, Stanford University, CA 94305, USA

Abstract

Flow effects on chemical reactions at a solid-liquid interface are fundamental to diverse technological applications but remain poorly understood from a molecular perspective. In this work, we demonstrate that the coupling between laminar flow and surface chemistry can be adequately described using the classical density functional theory for ion distributions near the surface in conjunction with kinetics modeling and the Navier-Stokes equation. In good agreement with recent experiments, we find that flowing of fresh water over a silica surface may result in drastic changes in the rate of silica dissolution and, consequently, the surface charge density and the interfacial structure. A nonlinear streaming current is predicted when the surface reactions are disturbed by a laminar flow.

* Email: jwu@engr.ucr.edu or hlliu@ecust.edu.cn

TOC Graphic

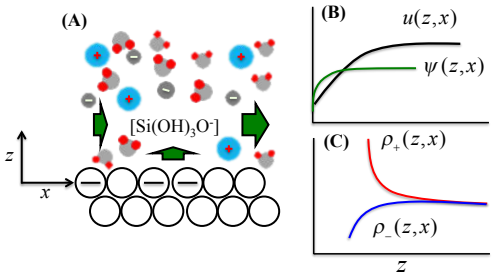

1. Introduction

Understanding the interfacial properties of aqueous solutions in contact with solid surfaces has been actively pursued in various fields of scientific studies, including surface sciences[1-3], electrochemistry[4-6], catalysis[7, 8], colloid science[9, 10], molecular cell biology[11], and geochemistry[12, 13]. The interfacial structure and chemical reactions taking place at a solid surface are dependent on a wide spectrum of physicochemical parameters[12, 14, 15]. While conventional studies are mostly focused on the influences of thermodynamic conditions such as temperature, pH, and the chemical composition on the interfacial behavior, relatively little is known on how the liquid flow over the interface affects the local solution conditions and surface reactions. A faithful description of the flow effects is important for design and optimization of a broad range of electrochemical and geochemical processes ranging from ionic motions in different electrochemical and microfluidic devices to hydraulic fracturing and carbon dioxide sequestration.

An inorganic solid in contact with an aqueous solution often bears an electrostatic charge at the surface due to various physiochemical processes such as ion dissolution, substitution and chemical adsorption. The surface charge, along with mobile ions in the aqueous solution, forms an electric double layer (EDL), which plays a dominant role in the interfacial behavior. A conventional wisdom is that neither the EDL structure nor the surface reactivity will be significantly influenced by the solution flow over the solid surface. While there have been a number of previous investigations on the coupling between surface reactions, flow-driven transport and electric double layer structure[16-19], a recent experimental study based on surface-specific sum frequency generation spectroscopy (SFG) and microfluidics indicates that a rapid laminar flow may lead to the reversible modification of the surface charge and, subsequently, realignment of the interfacial water molecules[1]. The coupling between flow dynamics, EDL

structure and surface chemistry is not unexpected in the presence of a strong flow but such effects are typically ignored in conventional models of electrokinetic phenomena[20-24].

In this work, we investigate the flow effects on the surface structure and reactivity using a theoretical procedure that combines the classical density functional theory (CDFT) for ion distributions, kinetic modeling of the surface reactions, and the Navier-Stokes equation for the fluid velocity. The new theoretical framework takes into account not only electrostatic correlations and ion size effects that are ignored in the conventional space-charge model but also coupling effects between surface reactions, ion distributions and the electroosmotic flow. The theoretical predictions are found in good agreement with the SFG detection of the surface charge density. The implications of flow-induced surface reactions on the EDL structure and the streaming current are also discussed.

2. Model System and Theoretical Methods

Consider a laminar flow for an aqueous electrolyte solution through a rectangular silica channel of height H in nanoscale but both width w and length L in macroscopic dimensions. The microfluidic setup was commonly used in previous studies of surface reaction and ion flow by theoretical or experimental means[25]. As shown schematically in Figure 1, the aqueous solution flows along the silica surface driven by a pressure gradient ∇P. Although SiO_2 solubility in water is extremely small, the surface bears a negative charge when the solution pH is higher than the point of zero charge (pzc), i.e., the pH value at which the surface is electrostatically neutral. The pzc value is about pH=2 for a fused silica surface[26].

In the presence of an electrolyte solution, the silica charge density dictates ion distributions as well as the orientation of water molecules near the surface. In addition to pH, the surface charge density can be influenced by the electrolyte concentration in the bulk (Fig. 1b) and the local solvent

velocity (Fig. 1c). As illustrated in Figure 1, the surface charge density and the local ion distributions are coupled with the electroosmotic flow through the kinetics of surface reactions.

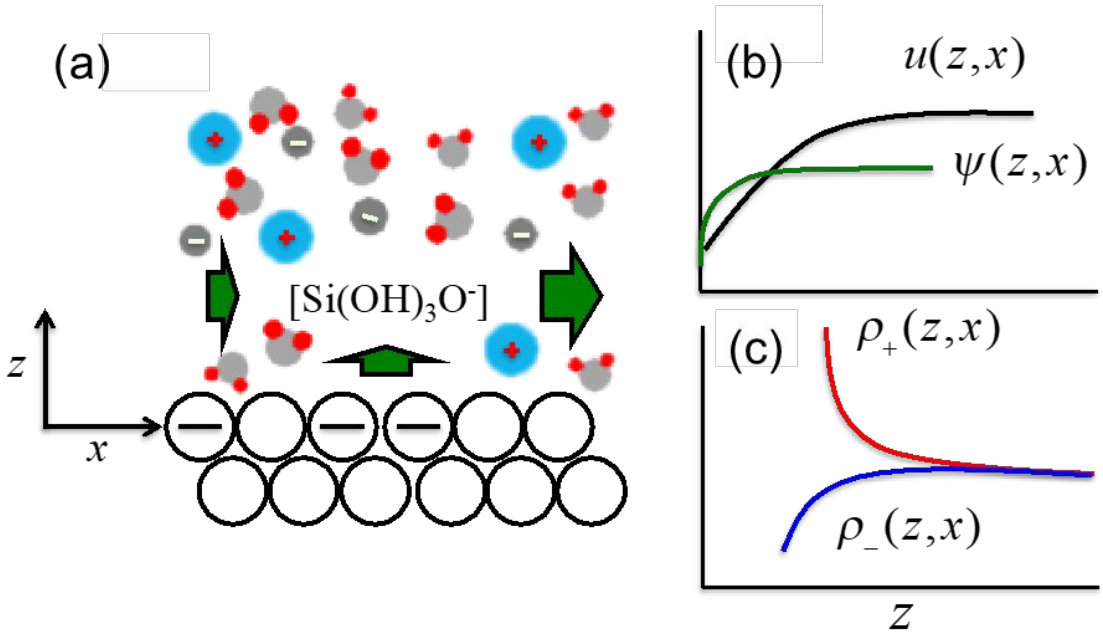

Figure 1 (a) A schematic view of an aqueous solution flowing along a fused silica surface. The flow affects the surface reaction kientics and charge density, the electric double layer (EDL) structure, and ion transport, which in terms influence the solvent velocity. (b) A qualitative description of local electrostatic potential $\psi(z,x)$ and solvent velocity $u(z,x)$. (c) The electric double layer struture as represented by the local density of counterions, $\rho_{+}(z,x)$, and the local density of coions, $\rho_{-}(z,x)$.

For fused silica in an aqueous solution, the surface charge arises from dissolution and deprotonation reactions[1, 3, 27-30]. When for pH>pzc, SiO_2 dissolution is dominated by the hydrolysis of the Si-O-Si bond

$$\equiv \text{Si-O-Si(OH)}_2\text{O}^- + \text{H}_2\text{O} \underset{k_{-1}}{\overset{k_{+1}}{\rightleftharpoons}} \equiv \text{Si-OH} + \text{Si(OH)}_3\text{O}^-(\text{aq}) \qquad (2)$$

where "$\equiv$" denotes the connection of a chemical group with the solid surface, k_{+1} and k_{-1} stand for the rates of forward and backward reactions, respectively. A similar equation can be written for the deprotonation of silanol groups at the surface:

$$\equiv \text{Si-OH} \underset{k_{-2}}{\overset{k_{+2}}{\rightleftharpoons}} \equiv \text{Si-O}^- + \text{H}^+(\text{aq}) \tag{3}$$

The surface reactions are different when pH<pzc. In that case, silica hydrolysis has little effect on the surface charge density.

We can calculate the surface charge density based on the overall concentrations of $\equiv$ Si-O$^-$ and $\equiv$ Si-O-Si(OH)$_2$O$^-$ residues at the silica surface:

$$Q = -e\left(N_{\equiv \text{Si-O}^-} + N_{\equiv \text{Si-O-Si(OH)}_2\text{O}^-} \right) \tag{4}$$

where $e = 1.602 \times 10^{-19}$ C is the unit charge, $N_{\equiv \text{Si-O}^-}$ and $N_{\equiv \text{Si-O-Si(OH)}_2\text{O}^-}$ stand for the number densities of $\equiv$ Si-O$^-$ and $\equiv$ Si-O-Si(OH)$_2$O$^-$ groups at the surface, respectively. For a given silica surface, the number density of silicon atoms includes contributions from three types of functional groups,

$$N_{total} = N_{\equiv \text{Si-OH}} + N_{\equiv \text{Si-O}^-} + N_{\equiv \text{Si-O-Si(OH)}_2\text{O}^-} \ . \tag{5}$$

While the total number density is fixed, the number density of silicon atoms in each functional group may change due to surface reactions.

As the total number density of different silicon functional groups N_{total} is not affected by surface reactions, it can be shown that, at the steady-state condition, the surface charge density is related to the surface electrical potential ψ_0, the bulk pH, and the Si(OH)$_3$O$^-$ concentration in the bulk, $C_{\text{Si(OH)}_3\text{O}^-}$. From Eq.(1)~(5), we could obtain the expression of surface charge density:

$$Q = -eN_{total} \frac{k_2 10^{-pH} \exp(-\beta e\psi_0) - k_{-1} C_{\text{Si(OH)}_3\text{O}^-}}{k_2 + k_{-2} 10^{-pH} \exp(-\beta e\psi_0) - k_1 - k_{-1} C_{\text{Si(OH)}_3\text{O}^-}} \tag{6}$$

where $\beta = k_B T$, k_B is Boltzmann constant, and T is the temperature. In writing Eq.(6), we have utilized the condition of mass balance for ≡ Si-OH

$$k_{+1} N_{\equiv \text{Si-O}^-} - k_{-1} N_{\equiv \text{Si-OH}} C_{\text{Si(OH)}_3\text{O}^-} = k_{-2} N_{\equiv \text{Si-O}^-} C_{\text{H}^+} - k_{+2} N_{\equiv \text{Si-OH}} \tag{7}$$

and the Boltzmann equation for the proton ion concentration at the silica surface.

In the presence of a laminar flow, $\text{Si(OH)}_3\text{O}^-$ ions dissolve from the solid surface leading to an increase of silica concentration along the flow direction. At the steady-state condition, the rate of $\text{Si(OH)}_3\text{O}^-$ dissolution per unit area, R_D, is balanced by the change in the rate of mass convection

$$R_D = k_{+1} N_{\equiv \text{Si-O}^-} - k_{-1} N_{\equiv \text{Si-OH}} C_{\text{Si(OH)}_3\text{O}^-} = \frac{C_{\text{Si(OH)}_3\text{O}^-}}{2L} \int_0^{H/2} u(z)\, dz \tag{8}$$

where $u(z)$ stands for the average flow velocity, and L is the length in the nanochannel. In writing Eq.(8), we assume that $C_{\text{Si(OH)}_3\text{O}^-}$ is uniform in the direction perpendicular to the surface. Assuming a linear variation of the surface charge density in the flow direction, we can rewrite Eq.(7) in terms of the average surface charge density and ion concentrations.

To find the solvent (water) velocity near the pore surface, we use the Navier-Stokes (NS) equation

$$\eta \frac{\partial^2 u}{\partial z^2} - \rho_e(z) \frac{\partial \psi}{\partial x} - \frac{\partial P}{\partial x} = 0 \tag{9}$$

where $u(z)$ stands for the velocity profile in the direction perpendicular to the surface z, η represents the solvent viscosity, $\rho_e(z)$ represents the local charge density of the aqueous solution, $\partial\psi / \partial x$ and $\partial P / \partial x$ are the gradients of the electric potential and pressure in the flow direction (x-direction), respectively. The local charge density is related to the local concentrations of ions

$$\rho_e(z) = \sum_i Z_i e \rho_i(z) \tag{10}$$

where Z_i is the valence of i^{th} ionic species. For all systems considered in this work, we have $\partial\psi / \partial x = 0$ and $\partial P / \partial x$ is a constant. As a result, we can solve the velocity profile near the surface analytically by using the following boundary conditions (BCs)

$$\begin{cases} bu(z)' = u(0), & \text{at z} = 0 \\ u(z)' = 0, & \text{at z} = \infty \end{cases} \tag{11}$$

where b represents the slip length for water flowing along the solid surface. In general, the slip length is negative if the surface is hydrophilic and positive if it is hydrophobic[31]. Here the slip length has relatively small effects on ion transport and electric current, and $b = 0$ is adopted for all calculations in this work.

With the assumption of local equilibrium in the direction perpendicular to the surface, the ion density distributions in the electric double layer (EDL) can be predicted from CDFT[24, 32-34]. The thermodynamic method calculation is based on the primitive model for electrolyte solutions whereby all ions are treated as charged hard spheres and the solvent is modeled as a dielectric continuum[35]. The ion density profile is given by

$$\rho_i(z) = \rho_i^{bulk} \exp\left[-\beta Z_i e \psi(z) - \beta \Delta\mu_i^{ex}(z) \right] \tag{12}$$

where ρ_i^{bulk} stands for the bulk concentration for the i^{th} type ion, $\psi(z)$ is the local electric potential at position z, and $\Delta\mu^{ex}(z)$ corresponds to the deviation of the local excess chemical potential from that corresponding to the bulk system. In the Poisson-Boltzmann equation (PB) or the space-charge model, $\Delta\mu^{ex}(\text{z})$ is ignored so that they are not able to account for the effects of electrostatic correlations and ionic excluded volumes. The local excess chemical potential $\Delta\mu^{ex}(z)$ includes a contribution from the modified fundamental measure theory (MFMT)[36] to account for excluded

volume effects of ions, and a second-order perturbation theory for electrostatic correlations[37]. The details of CDFT for inhomogeneous ionic systems could be found in our previous work[35-37]. Throughout this work, the diameters of hydrated cations and anions are set to 0.5 nm, which is reasonable for an aqueous NaCl solution. At the ambient temperature, the dielectric constant for liquid water is ε_r=78.4.[4]

We can solve for the ion distributions and the local electric potential self-consistently from the Poisson Equation

$$\frac{d^2\psi(z)}{dz^2} = -\frac{4\pi e}{\varepsilon_0 \varepsilon_r}\rho_e(z) \tag{13}$$

with the boundary conditions

$$\psi(0) = \psi(H) = \psi_0 \tag{14}$$

$$\left.\frac{\partial\psi(z)}{\partial z}\right|_{z=\frac{H}{2}} = 0 \ . \tag{15}$$

Here ε_0 = 8.8542×10^{-12} F/m is the vacuum permittivity, ε_r=78.4 is the water dielectric constant.

In the absence of ion flow, the surface charge density on the wall can be obtained according to the electrostatic neutrality

$$Q = -\varepsilon_0 \varepsilon_r \left.\frac{\partial\psi(z)}{\partial z}\right|_{z=0} . \tag{16}$$

In that case, we can estimate the total number density of the silicon atoms at the surface N_{total} as well as the kinetic constants for the surface reactions based on experimental data for the surface charge density. Given a pressure gradient, the velocity profile can be solved from Eq.(9). Subsequently, the ionic density profiles $\rho_i(z)$, the surface charge density Q, and the local electrical potential $\psi(z)$ throughout the pore could be calculated from Eqs.(12)-(13) in

conjunction with the boundary conditions shown in Eqs.(14)-(15) and the kinetic model for surface reactions, Eq.(6).

For a laminar flow through a silica nanochannel of height H in nanoscale and width w and length L in macroscopic dimensions, the streaming current arises from primarily the convective flow dragging the excess counterions at top and bottom surfaces of the channel. Based on the ionic density profiles in the slit pore, we can calculate the total streaming current[38]

$$I_{str} = w\int_0^H \sum_i Z_i e\rho_i(z)u_i(z)dz\,. \tag{17}$$

while $u_i(z) = u(z)$ is the velocity of i^{th} ion at different positions. Because $w >> H$, we assume that the sidewall effects may be ignored and that the solvent velocity and the ion density profiles can be treated as uniform along the direction of the flow (*viz*., ion diffusion in the flow direction is neglected).

3. Results and Discussions

We first consider the surface charge density for a silica nanochannel (height H =29nm, width w=5.8μm, the length L = 40μm) in contact with an aqueous NaCl without flow at the concentration of 0.01 M. Because the EDL thickness is much smaller than the channel height, the surface charge density of the nanochannel is expected to be identical to that of a planar silica surface. As a result, the theoretical results can be directly calibrated with experimental data.

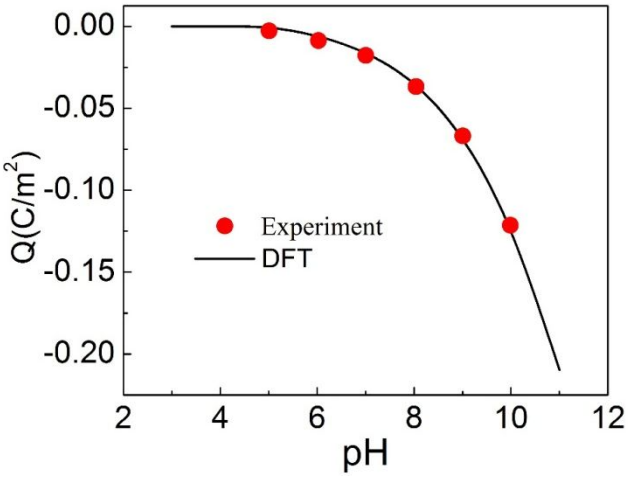

Figure 2 Surface charge density Q of SiO_2 substrate versus pH without flow. The line is predicted by CDFT and these points are experimental results[39]. The bulk NaCl concentration is 0.01 M.

Figure 2 shows the dependence of the surface charge density on pH from the theoretical calculations in comparison with experiment for a planar silica surface[39]. Here N_{total} = 8 nm^{-2} is estimated according to the surface structure of SiO_2, and the kinetic constants, k_{+1}=1×10^{-6} s^{-1}, k_{-1}=3×10^{-4} s^{-1} M^{-1}, k_{+2}=5×10^{-12} s^{-1}, k_{-2} =2.2×10^{-4} s^{-1}M^{-1}, are obtained by fitting the relation between surface charge density and pH shown in Figure 2. The fitting parameters are subject to the constraints of equilibrium constants that are also known experimentally (K_1=k_{+1}/k_{-1}, K_2=k_{+2}/k_{-2}). Apparently, the simple kinetic model is able to capture the experimental data quantitatively. In addition, the kinetic parameters is well agreed with the relaxation time of silica surface[1]. As the solution pH increases, more negatively charged SiO^- are dissociated from the functional groups SiOH resulting in a more negative surface charge density.

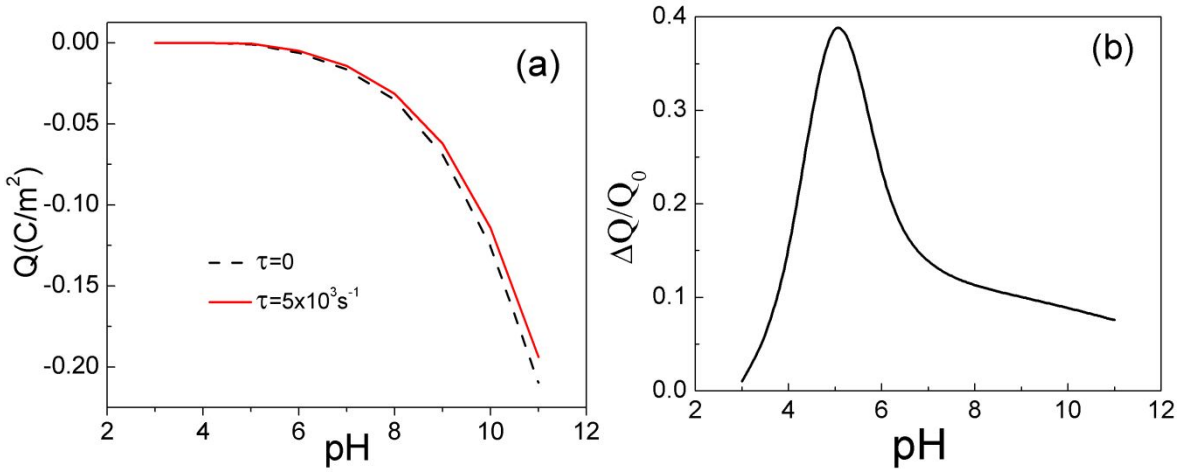

Figure 3 Flow effect on the surface charge density. (a) Surface charge density versus pH with or without flow effect. (b) Flow effect on the change of surface charge density under different pH.

Figure 3a shows the flow effect on the surface charge density. The presence of a laminar flow (shear rate = 5×10^3 s^{-1}) reduces surface charge density, in particular at high pH. According to Eq. (2), the SiO_2 surface is negative for pH>3 as the hydrolysis leads to the negative surface charge. Without the flow, the effective forward and backward reaction rates are balanced with each other, i.e., the solution near the surface is saturated with silicic acid. The flow reduces the silicic acid concentration near the surface by introducing fresh water, driving the dissociation equilibrium toward the right side of Eq. (2). This effectively removes negative charges from the surface and thereby lowering the surface charge density. However, the subsequent deprotonation of the newly formed neutral Si-OH surface state in Eq.(3) restores the negative surface charge. These two competing reactions establish a steady state with a reduced surface charge.

The change of the surface charge density is shown in Figure 3(b). Here $\Delta Q=Q-Q_0$ is the difference between that with and that without flow Q_0, i.e., the surface charge density for water at rest. The relative change of surface charge density displays a maximum at pH=4~6 due to the flow effect.

Although the flow effect is most significant at large pH, the absolute value of the surface charge density also increases.

The results shown in Figure 3 can help understand the flow effect on the sum frequency generation spectroscopy (SFG) intensity at SiO_2 surface[1]. The magnitude of the SFG signal reflects the degree of alignment of water molecules due to the electrostatic field at the surface, which is mainly influenced by the change in relative surface charge density. At both low and high pH (pH=3 or 11), the reduction in SFG intensity upon flow is very small; it shows a maximum at pH=6.5 when the flow effect on the fluctuation of water orientations is most significant.

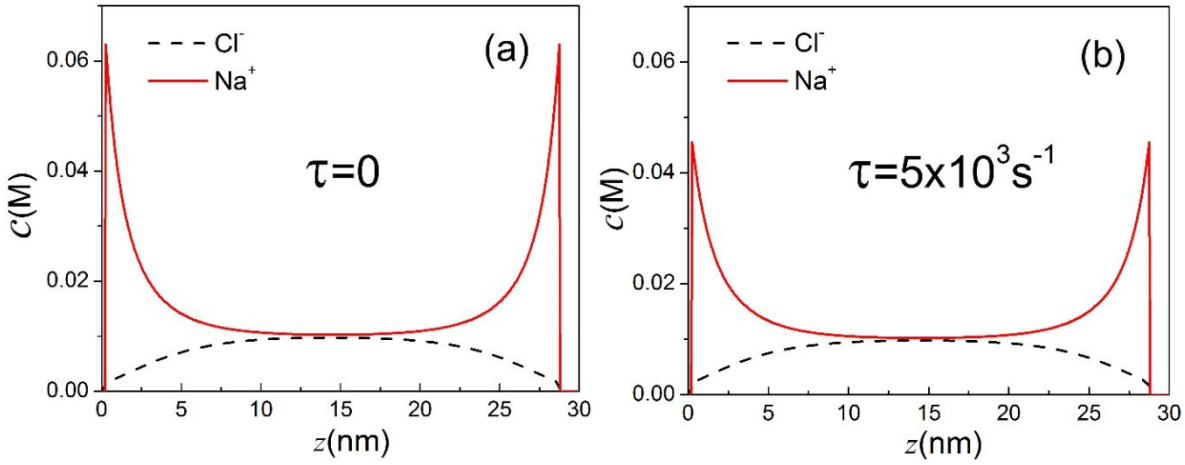

Figure 4 Flow effect on the EDL structure at pH=6.5 (a) without flow and (b) under a flow with the shear rate of 5×10^3/s.

As discussion above, flowing an eletrolyte solution over a surface can change the surface reactions and thus the surface charge density. The latter is related not only to the EDL structure but also to the alignment of water molecules in terms of both the degree of water orientation and fluctutations. Figure 4(a) shows the EDL structure of the SiO_2-water interface at pH=6.5 when the water is at rest, and Figure 4 (b) presents EDL structure under a flow with the shear rate of 5×10^3/s. The flow reduces the surface charge density and thus the contact density of cations near

the silica surface. The flow effect on the density profile of Cl^- ions is relatively insignificnat probably because the surface charge is screened by Na^+ ions and the change in the surface charge density is closely affiilated with the dissociation of $Si(OH)_3O^-$ ions.

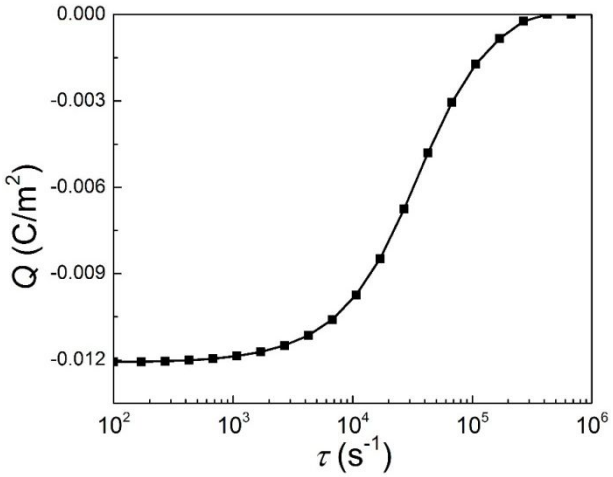

Figure 5 Surface charge density Q of SiO_2 substrate versus the pressure drop. Here the nanotube height H=29nm, width w=5.8μm the length L = 40μm. The bulk concentration of NaCl is 0.01M and pH=6.5.

Figure 5 shows the surface charge density of SiO_2 substrate versus the shear rate (pressure drop) when pH is 6.5. When the shear rate is less than 1×10^3 s^{-1}, the surface charge density almost remains the same because the slow flow cannot significantly alter the concentration of silicic acid which determins the surface chemical reactions. However, the flow with a high shear rate (larger than 1×10^3 s^{-1}) causes a very large decrease in the surface charge density. With the extremely high shear rate, which might be difficult to archieve in real experiments, the surface charge density decreases almost to zero. In that extreme case, the flow washs away essentially all silicic acid molecules near the surface, and the reaction in Eq.(2) dominates the surface reaction.

As discussed above, a streaming current is induced by application of a pressure gradient across a charged channel, which can be calculated from the ion density profiles and velocities. The conventional equation for the streaming current is given by[40]

$$I_{str} = \frac{\varepsilon_0 \varepsilon_r \zeta A}{\eta}(\Delta P / L) \tag{18}$$

where ζ is the zeta potential, A and L are the cross-section area and the length of the channel, respectively. Without surface reactions, ζ is a constant, thus Eq.(18) predicts a linear relationship between the stream current and the pressure gradient[41]. A number of recent publications indicate that Eq.(18) may break down due to various non-slippery boundary conditions[42-46]. However, it remains unclear how the streaming current is affected when surface reactions are coupled with the flow. Many factors can cause the non-linear streaming conductance phenomenon[42-46], could the linear streaming current phenomenon be affected by surface reactions?

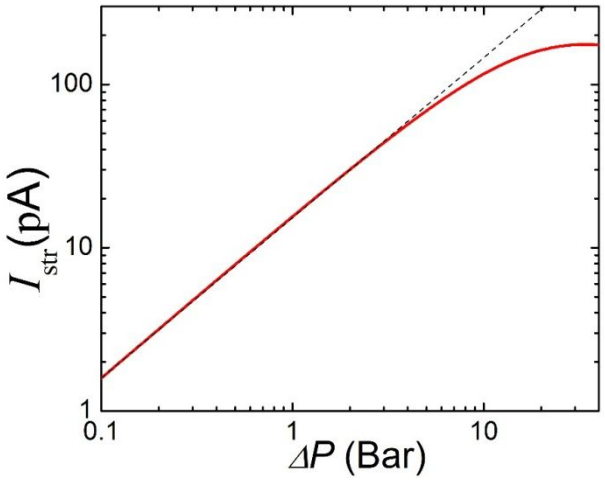

Figure 6 Dependence of streaming current on the pressure drop for SiO_2 substrate. Here the nanotube height H =29 nm, width w=5.8 μm the length L = 40μm. The bulk salt concentration is 0.01M and pH=6.5.

Figure 6 shows the streaming current as a function of applied pressure. I_{str} increases linearly with applied pressure under ~3 bars. As discussed above, with flow effect on pore surface reactions, the negative surface charge density decreases thus decreasing the streaming. While Eq.(17) predicts that the streaming current is linearly proportional to the pressure gradient of the channel, we find a non-linear streaming current phenomenon in a single nanopore by condsidering the flow effect on the chemical reactions of pore surface when the driven pressure is very large.

4. Conclusions

In summary, the flow effects on surface chemical reactions at solid-liquid interface could be quantitatively described with classical DFT plus conventional equations of fluid mechanics and reaction kinetics. The theoretical results show that the solvent flow over a solid surface can dramatically change the rate of surface reactions and subsequently the surface charge density and the EDL structures. Because the flow influences the surface charge density, the surface reactions perturbed by the flow lead to a nonlinear streaming current at high driven pressure. It is our hope that this work provides a better understanding of the coupling effects of surface reactions, EDL structure and flow behavior that is essential for a faithful description of transport phenomena near solid surfaces including ion mobility in the micropores of electrode materials.

5. Acknowledgements

Inspiring discussions with David J. Wesolowski is gratefully acknowledged. This work was sponsored by the National Natural Science Foundation of China (No. 91834301, 91534202, 21808055), National Natural Science Foundation of China for Innovative Research Groups (No. 51621002), and the 111 Project of China (No. B08021). We also thank the Project funded by China Postdoctoral Science Foundation (2017M620137), Shanghai Sailing Program (18YF1405400), Fundamental Research Funds for the Central Universities (WJ1814016), and the National Postdoctoral Program for Innovative Talents (BX201700076). Jianzhong Wu thanks the financial support by the Fluid Interface Reactions, Structures and Transport (FIRST) Center, an Energy Frontier Research Center funded by the U.S. Department of Energy, Office of Science, Office of Basic Energy Sciences.

6. Reference

1. D. Lis, E. H. Backus, J. Hunger, S. H. Parekh and M. Bonn, *Science*, 2014, **344**, 1138-1142.

2. E. Secchi, A. Niguès, L. Jubin, A. Siria and L. Bocquet, *Physical Review Letters*, 2016, **116**, 154501.

3. J. Schaefer, E. H. Backus and M. Bonn, *Nature Communications*, 2018, **9**, 3316.

4. V. Augustyn, J. Come, M. A. Lowe, J. W. Kim, P.-L. Taberna, S. H. Tolbert, H. D. Abruna, P. Simon and B. Dunn, *Nature Materials*, 2013, **12**, 518-522.

5. V. Presser, C. R. Dennison, J. Campos, K. W. Knehr, E. C. Kumbur and Y. Gogotsi, *Advanced Energy Materials*, 2012, **2**, 895-902.

6. C. Lian, K. Liu, K. L. Van Aken, Y. Gogotsi, D. J. Wesolowski, H. L. Liu, D. E. Jiang and J. Z. Wu, *ACS Energy Letters*, 2016, **1**, 21-26.

7. M. Cargnello, V. V. Doan-Nguyen, T. R. Gordon, R. E. Diaz, E. A. Stach, R. J. Gorte, P. Fornasiero and C. B. Murray, *Science*, 2013, **341**, 771-773.

8. J. Di, C. Zhu, M. Ji, M. Duan, R. Long, C. Yan, K. Gu, J. Xiong, Y. She, J. Xia, H. Li and Z. Liu, 2018, **130**, 15063-15067.

9. J. Zeng, X. Xia, M. Rycenga, P. Henneghan, Q. Li and Y. Xia, *Angewandte Chemie International Edition*, 2011, **50**, 244-249.

10. H. Su, A. A. Barragan, L. Geng, D. Long, L. Ling, K. N. Bozhilov, L. Mangolini and J. J. A. C. Guo, 2017, **129**, 10920-10925.

11. S. Buyukdagli, R. Blossey and T. Ala-Nissila, *Physical review letters*, 2015, **114**, 088303.

12. A. Putnis, *Science*, 2014, **343**, 1441-1442.

13. D. Wang, S. C. Pillai, S.-H. Ho, J. Zeng, Y. Li and D. D. Dionysiou, *Applied Catalysis B: Environmental*, 2018, **237**, 721-741.

14. G. E. Brown, V. E. Henrich, W. H. Casey, D. L. Clark, C. Eggleston, A. Felmy, D. W. Goodman, M. Grätzel, G. Maciel and M. I. McCarthy, *Chemical Reviews*, 1999, **99**, 77-174.

15. C. Lian, H. Liu, C. Li and J. Wu, *AIChE Journal*, 2019, **DOI:10.1002/aic.16467**, DOI:10.1002/aic.16467.

16. S. Qian and J. F. L. Duval, *Journal of Colloid and Interface Science*, 2006, **300**, 413-428.

17. J. F. L. Duval, E. Sorrenti, Y. Waldvogel, T. Görner and P. De Donato, *Physical Chemistry Chemical Physics*, 2007, **9**, 1713-1729.

18. S. Qian and J. F. L. Duval, *Journal of Colloid and Interface Science*, 2006, **297**, 341-352.

19. J. F. L. Duval, M. Minor, J. Cecilia and H. P. van Leeuwen, *The Journal of Physical Chemistry B*, 2003, **107**, 4143-4155.

20. G. A. Waychunas, *Science*, 2014, **344**, 1094-1095.

21. L.-H. Yeh, S. Xue, S. W. Joo, S. Qian and J.-P. Hsu, *The Journal of Physical Chemistry C*, 2012, **116**, 4209-4216.

22. Y. Qiu, Q. Tan, W. Si and Y. Chen, *Science China Technological Sciences*, 2014, **57**, 230-238.

23. B. L. Werkhoven, J. C. Everts, S. Samin and R. van Roij, *Physical Review Letters*, 2018, **120**, 264502.

24. C. Lian, A. Gallegos, H. Liu and J. J. P. C. C. P. Wu, 2017, **19**, 450-457.

25. A. Rimola, D. Costa, M. Sodupe, J. F. Lambert and P. Ugliengo, *Chemical Reviews*, 2013, **113**, 4216-4313.

26. V. Ostroverkhov, G. A. Waychunas and Y. R. Shen, *Chem Phys Lett*, 2004, **386**, 144-148.

27. A. Seidel, M. Löbbus, W. Vogelsberger and J. Sonnefeld, *Solid State Ionics*, 1997, **101**, 713-719.

28. F. Nikaido, S. Inasawa, Y. Tsuji and Y. Yamaguchi, *Bulletin of the Chemical Society of Japan*, 2013, **86**, 520-525.

29. M. Barisik, S. Atalay, A. Beskok and S. Qian, *The Journal of Physical Chemistry C*, 2014, **118**, 1836-1842.

30. J. Škvarla, *Langmuir*, 2007, **23**, 5305-5314.

31. L. Bocquet and E. Charlaix, *Chemical Society Reviews*, 2010, **39**, 1073-1095.

32. J. Wu, *AIChE journal*, 2006, **52**, 1169-1193.

33. J. Wu and Z. Li, *Annu. Rev. Phys. Chem.*, 2007, **58**, 85-112.

34. C. Lian, K. Liu, K. L. Van Aken, Y. Gogotsi, D. J. Wesolowski, H. L. Liu, D. E. Jiang and J. Z. Wu, *ACS Energy Letters*, 2016, DOI: 10.1021/acsenergylett.6b00010, 21-26.

35. X. Kong, J. Jiang, D. Lu, Z. Liu and J. Wu, *The Journal of Physical Chemistry Letters*, 2014, **5**, 3015-3020.

36. J. G. Ibarra-Armenta, A. Martin-Molina and M. Quesada-Perez, *Phys Chem Chem Phys*, 2011, **13**, 13349-13357.

37. Z. D. Li and J. Z. Wu, *Journal of Physical Chemistry B*, 2006, **110**, 7473-7484.

38. M.-S. Chun, M. S. Shim and N. W. Choi, *Lab on a Chip*, 2006, **6**, 302-309.

39. A. Kitamura, K. Fujiwara, T. Yamamoto, S. Nishikawa and H. Moriyama, *Journal of nuclear science and technology*, 1999, **36**, 1167-1175.

40. S. Wall, *Current Opinion in Colloid & Interface Science*, 2010, **15**, 119-124.

41. A. Delgado, F. González-Caballero, R. Hunter, L. Koopal and J. Lyklema, *Pure and Applied Chemistry*, 2005, **77**, 1753-1805.

42. Y. Xie, L. Wang, M. Jin, Y. Wang and J. Xue, *Applied Physics Letters*, 2014, **104**, 033108.

43. R. Saini, A. Garg and D. P. Barz, *Langmuir*, 2014, **30**, 10950-10961.

44. J. Hoffmann and D. Gillespie, *Langmuir*, 2013, **29**, 1303-1317.

45. L. Joly, F. Detcheverry and A.-L. Biance, *Physical Review Letters*, 2014, **113**, 088301.

46. A. Siria, P. Poncharal, A.-L. Biance, R. Fulcrand, X. Blase, S. T. Purcell and L. Bocquet, *Nature*, 2013, **494**, 455-458.